Scatterer detection by successive cancellation for UWB - method and experimental verification

Santos, Telmo; Kåredal, Johan; Almers, Peter; Tufvesson, Fredrik; Molisch, Andreas

Published in:
[Host publication title missing]

DOI:
10.1109/VETECS.2008.104

2008

Scatterer Detection by Successive Cancellation for UWB - Method and Experimental Verification

Telmo Santos,* *Student Member, IEEE*, Johan Karedal,* *Student Member, IEEE*, Peter Almers,*
Fredrik Tufvesson,* *Senior Member, IEEE*, Andreas F. Molisch,*† *Fellow, IEEE*
*Department of Electrical and Information Technology, Lund University, Sweden
†Mitsubishi Electric Research Laboratories (MERL), Cambridge, MA, USA

***Abstract*— We present a new high delay resolution method to detect Ultra-Wideband (UWB) scatterers when using frequency domain measurements. Our approach makes use of the impulse response envelope amplitudes and delays measured over a distance that is larger than the region of stationarity, and detects the 2-D coordinates of the channel scatterers, assuming that only single-scattering (single-interaction) processes occur. The identification methodology is based on multiple application of interference cancellation: at every step, we detect the strongest scatterer from an array of measurements, save its information, cancel it from the channel and search for the next strongest scatterer. To precisely define the strength of each scatterer, we present a method to define its *birth* and *death* locations along the measurement array. Finally, we verify the method by applying it to measurement results in an outdoor environment; the scatterer locations identified from the measurements show excellent agreement with the physically present objects like walls and columns.**

I. Introduction

The identification and characterization of scatterers is crucial for many aspects of wireless communications, including channel modeling, ranging, and automated creation of environment maps. Sounding of the channel with UWB signals is especially promising due to their fine delay resolution. The unlicensed and commercially available bandwidth of 7.5 GHz (3.1-10.6 GHz) leads to a delay resolution of 133 ps, which in turn, enables the detection of more scatterers than in narrowband systems.

Because of its importance, scatterer detection has been investigated by a considerable number of papers in the past. We can roughly distinguish three categories

- Localization and imaging methods for UWB: e.g., [1] where an array of receive antennas is used to track the position of the transmit antenna. The position estimation is based on time-of-flight similarly to our method. Furthermore, the measured data is used to create an image of the surrounding environment. This differs from our approach in the sense that we aim to find the exact position of channel scatterers and not to create and image of the whole environment.
- Channel estimation for narrowband measurements: e.g., [2] where the spatial location of clusters is found by means of high resolution multi-dimensional parameter estimation algorithms. The drawback of such methods is the high computational effort. Also, the limited bandwidth of the measurement means that especially closely spaced scatterers are difficult to resolve.
- Channel estimation for UWB measurements: more complex UWB channel estimation algorithms as the UWB-SAGE [3] (for frequency domain channel sounding) and the Sensor-CLEAN algorithm [4] (for time domain channel sounding) can also be used to perform the detection in an accurate way. These algorithms are, in general, computationally more complex than the one presented here.

In this paper, we propose a new high-resolution algorithm that is based on UWB synthetic array measurements (a synthetic array is generated by measuring with a single antenna at a number of different locations). Our algorithm has some similarities to both the CLEAN algorithm and UWB-SAGE in that it uses successive interference cancellation. The key distinction is that we propose the measurement points to cover distances *larger than the region of stationarity*.[1] This is in contrast to the above mentioned methods, which use measurement points in small grids within stationarity regions. We believe that using larger measurement distances covering several areas of stationarity, enables the identification of more scatterers in a more accurate fashion. One of the reasons for this, lies on the fact that the wavefronts arriving to the array are spherical and therefore it becomes easier to focus on the spatial points which originated them.

In this method we aim mainly to identify the exact delays corresponding to the channel scatterers and map them to points in space with two dimensional coordinates, assuming that only single-scattering processes occur. The scatterer coordinates form the basis for geolocation and automatic generation of environment scatterer maps, which is a key area of research for search-and-rescue operations. The scatterer location is also very useful for physically-based channel modeling and helps in the extraction of parameters such as delay dispersion, mean power, arrival delays, visibility region (in respect to both space and time), etc.

We demonstrate the validity and accuracy of the method by analyzing real data measured in an outdoor scenario. The scatterer locations that we identified agree very well with actual physical objects in the environment.

The remainder of the paper is organized the following way: Section II describes the signal and channel model. Section III describes the details of the high-resolution algorithm. Section IV describes the evaluation of our outdoor measurements by means of the algorithm. A summary and conclusions wrap up the paper.

[1]By region of stationarity, we mean a region in space within which the channel scatterers maintain their absolute amplitude, but their delays are allowed to differ from position to position.

978-1-4244-1645-5/08/$25.00

II. Signal and Channel Model

In the most general case, the UWB channel impulse response is modeled as [5]

$$x(\tau) = \sum_{k=1}^{N} \alpha_k \chi_k(\tau) \otimes \delta(\tau - \tau_k), \tag{1}$$

where $\chi_k(\tau)$ denotes the distortion of the k^{th} echo due to the frequency selectivity of the interactions with the environment, N is the number of scatterers, α_k are their amplitudes and τ_k the corresponding delays (τ_k are such that $\tau_1 < \cdots < \tau_N$). However, this model can be applied for scatterer identification only if the distortion functions χ_k are known *a priori*. By using the simplified model as

$$x(\tau) = \sum_{k=1}^{L} \alpha_k \delta(\tau - \tau_k), \tag{2}$$

where L is the number of scatterers, a distorted pulse looks like a sequence of closely-spaced pulses with amplitudes given by the pulse distortion. Thus, the simplified model might ultimately identify more scatterers than the existing ones, but these will be closely spaced around the regions of the true scatterers.

The transmitter, receiver and scatterers, are defined by their two-dimensional Cartesian coordinates. The delay corresponding to k^{th} scatterer is found by calculating the propagation time corresponding to a wave traveling from the transmitter (P_{TX}) via the scatterer (S_k) to the receiver antenna (P_{RX}),

$$\tau_k = \left(d\left(P_{\text{TX}}, S_k\right) + d\left(S_k, P_{\text{RX}}\right)\right)/c. \tag{3}$$

The propagation speed is assumed to be the vacuum speed of light, $c \approx 3 \times 10^8$ m/s, i.e., slowing of waves by propagation through dielectric media is neglected.

The method that we aim to describe in this paper is based on frequency domain measurements. The data collected in such measurements are complex channel coefficients, one for each frequency point. Since our channel model is defined in the time domain, by (2), we can apply the Inverse Discrete Fourier Transform (IDFT) to our frequency domain data to obtain the equivalent channel impulse response,

$$x_r(\tau) = \frac{1}{N_F} \sum_{w=0}^{N_F-1} h_{r,w} e^{j2\pi(f_0 + w\Delta f)\tau}. \tag{4}$$

N_F is the total number of measured frequency points, f_0 is the lowest frequency and Δf is the frequency step. $h_{r,w}$ is the complex channel coefficient associated with the r^{th} array position and the w^{th} frequency point. Eq. (4) can also be defined in a vector notation by,

$$x_r(\tau) = \mathbf{p}(\tau)^T \mathbf{h}_r. \tag{5}$$

Here, $\mathbf{p}(\tau) \in \mathbb{C}^{N_F}$ is a vector of complex exponentials, constant for all array positions, $\mathbf{h}_r \in \mathbb{C}^{N_F}$ is composed by the coefficients of all the frequency points measured at one array position and $(\cdot)^T$ is the transpose operator. These vectors are defined as,

$$\mathbf{p}(\tau) = \left[\begin{array}{ccc} e^{j2\pi f_0 \tau} & \cdots & e^{j2\pi(f_0 + (N_F-1)\Delta f)\tau} \end{array}\right]^T \tag{6}$$

$$\mathbf{h}_r = \left[\begin{array}{ccc} h_{r,0} & \cdots & h_{r,N_F-1} \end{array}\right]^T. \tag{7}$$

Note that Eq. (5) is a continuous function, contrary to (2) which is only defined for discrete delays. In the next sections, we will describe how from (5) we arrive to (2) and make use of this data to identify the scatterers.

The total array size should, as possible, be several times greater than the expected stationarity region. Covering larger distances enables the detection of more scatterers in a more accurate way.

III. Method Description

The method for the scatterer detection is divided in four steps, and for the description of each, we dedicate one of the following subsections. The frequency domain measurements define step A. Then a high resolution peak search procedure is applied to the measured data, step B, followed by the weighting of all candidate scatterers, step C. Using those weights, the strongest scatterer is selected and canceled from the measured data, step D. The method is repeated from step B until a certain number of scatterers are found.

A. Measurement System and Setup

The method is based on measurements of the channel transfer function between TX and RX where the antenna position at one link end is fixed, while an array of antenna positions is used at the other link end. Measurements can be done, e.g., with a Vector Network Analyzer (VNA) capable of measuring the S_{21} parameter. The VNA, including cables and possible external amplifiers, must be properly calibrated. Here, the antennas are not included in the calibration and are thus seen as part of the channel. In order to accurately estimate the true strength (amplitude) of the scatterers, the azimuth pattern of the antennas should be as uniform as possible.

The measured data is written into a matrix,

$$\mathbf{H} = \left[\begin{array}{cccc} \mathbf{h}_1 & \mathbf{h}_2 & \cdots & \mathbf{h}_{N_R} \end{array}\right], \tag{8}$$

of size $(N_F \times N_R)$, where N_F and N_R are the number of measured frequency points and number of array positions, respectively. The column vector $\mathbf{h}_r$, corresponding to the r^{th} array position, is defined as in (7).

B. High Resolution Peak Search

The first step of the post processing procedure aims to identify the exact delays and envelope amplitudes of the most significant peaks of each one of the impulse responses along the array. We will successively identify the peaks, from the strongest to the weakest, using a *search and subtract* approach similar to [4] and [6], but adapted to our signal model.

For every fixed array position r, we start by estimating the delay at which the maximum of the envelope of the impulse response occurs,

$$\hat{\tau}_{r,l} = \arg\max_{\tau} \left|\mathbf{p}(\tau)^T \mathbf{h}_{r,l}\right|. \tag{9}$$

The subscript l identifies the l^{th} strongest peak. Then, with the knowledge of $\hat{\tau}_{r,l}$, we can find the corresponding complex amplitude,

$$\hat{\alpha}_{r,l} = \frac{\mathbf{p}(\hat{\tau}_{r,l})^T \mathbf{h}_{r,l}}{\mathbf{p}^T \mathbf{p}}. \tag{10}$$

and subtract the contribution from the total impulse response. In other words, the resolvable contributions are subtracted in multiple steps; at every step, $\mathbf{h}_{r,l}$ is calculated by,

$$\mathbf{h}_{r,l} = \begin{cases} \mathbf{h}_r & ,l = 1 \\ \mathbf{h}_{r,l-1} - \hat{\alpha}_{r,l-1}\mathbf{p}^*(\hat{\tau}_{r,l-1}) & ,l > 1 \end{cases}, \quad (11)$$

where $\mathbf{h}_r$ is the original, or measured, frequency transfer function and $(\cdot)^*$ denotes the conjugate. The process begins by setting $l = 1$ and it ends when a peak with amplitude $|\hat{\alpha}_{r,l}|$ is found below a predefined threshold, μ. The estimated delays and amplitudes are saved in appropriate vectors,

$$\hat{\mathbf{d}}_r = \begin{bmatrix} \hat{\tau}_{r,1} & \cdots & \hat{\tau}_{r,l_{\max}} \end{bmatrix}^T \quad (12)$$

$$\hat{\mathbf{a}}_r = \begin{bmatrix} |\hat{\alpha}_{r,1}| & \cdots & |\hat{\alpha}_{r,l_{\max}}| \end{bmatrix}^T, \quad (13)$$

for $r = 1, \ldots, N_R$. Since this procedure is performed independently for each array position, different positions can have a different number of detected peaks ($l_{\max}$ varies with r).

The process of finding the peak delays in (9) can be interpreted as Maximum Likelihood delay estimation problem where we try to estimate the parameter τ. In this paper, we will not address the problem of how to find this estimate. The simplest, but also more complex, way to find a reasonable estimate, is to perform a grid search with a step smaller than the delay resolution.

C. Weighing All Candidate Scatterers

The key innovation of our algorithm lies in merging together the information from all the array positions in order to clearly distinguish between the channel scatterers. For the scatterer detection we will continue to use a successive cancellation approach. Subsequently to the detection of the strongest scatterer, we cancel it from the channel and repeat the process to detect the next strongest scatterer.

The basis of the current step is the delays and amplitudes of the scatterers, as measured at the different locations. We then try to identify the geographical (2D Cartesian coordinates) location of the scatterers, and identify the locations where scatterers are "active". In other words, this step provides tracking of scatterers along the measurement rail, including their *birth* and *death* position.

In order to find the strongest scatterer, a search is performed over a two-dimensional grid, considering every geographical point as a candidate scatterer. The search step, i.e., distance between two consecutive points within the grid, must not exceed the system's spatial resolution, which inversely depends on the bandwidth, $d_{res} = c/\left(f_{\max} - f_{\min}\right)$. For each point on the grid we calculate the corresponding propagation delay for all array positions as defined in (3), assuming single scattering (single-interaction, single-bounce) paths. Then, to the k^{th} scatterer is assigned the vector of delays,

$$\mathbf{d}_k = \begin{bmatrix} \tau_{1,k} & \ldots & \tau_{N_R,k} \end{bmatrix}^T. \quad (14)$$

Now, for each array position r, we compare the scatterer delay $\tau_{r,k}$ with all the estimated peak delays in the corresponding vector $\hat{\mathbf{d}}_r$.[2] If there is a peak within the range of one delay resolution, we save the peak amplitude, if not, we set the amplitude to zero. The output is

$$\mathbf{a}_k = \begin{bmatrix} \alpha_{1,k} & \ldots & \alpha_{N_R,k} \end{bmatrix}^T, \quad (15)$$

where $\alpha_{r,k}$ can either be equal to $|\hat{\alpha}_{r,l}|$ (for a specific l) or zero, accordingly to the above criterion. Due to the ultrawideband nature of the channel, the delay of a specific scatterer generally differs for each measurement position. If a certain scatterer is a good candidate, then the corresponding vector (15) will have many non-zero elements (in the ensemble of all measurement positions), else, it will have only a few non-zero elements or be a vector of zeros.

At this point it is important to define the scatterers *birth* and *death* positions along the array, which is necessary because the measurement array covers more than one stationarity area. Then, we make use of these positions to calculate the scatterer strength.

To solve this problem, we apply an average sliding window (ASW) over the elements of the vector $\mathbf{a}_k$,

$$\mathbf{w}_k[r] = \frac{1}{N_W} \sum_{n=-N_W/2}^{N_W/2-1} \alpha_{n+r,k},$$

where N_W is the size of the sliding window and $r = 0, \ldots, N_R$. The value of N_W is set to be the number of array positions corresponding the stationarity area, thus depending on the scenario and on the size of the array step. The ASW is useful because it follows the overall trend of a certain scatterer along the array, not being influenced by the amplitude of a single peak. The limits (*birth* and *death*) of scatterer k are set by the ASW. A limit, is said to be found when $\mathbf{w}_k$ falls below the threshold μ, defined in step B. Finally, the strength of each scatterer is calculated as the sum of elements of $\mathbf{a}_k$, which are within the scatterer limits.

D. Detection and Cancellation of the Strongest Scatterer

Once all scatterer strengths are found, we find the strongest and save its information: strength, delays, selected peaks and spatial coordinates. Subsequently, we cancel this scatterer from the channel, and to do so, we make use of Eq. (11), for $L > 1$, once again

$$\mathbf{h}_r = \mathbf{h}_r - \hat{\alpha}_{r,l_{\text{peak}}}\mathbf{p}^*\left(\hat{\tau}_{r,l_{\text{peak}}}\right). \quad (16)$$

Here, $\alpha_{r,l_{\text{peak}}}$ and $\hat{\tau}_{r,l_{\text{peak}}}$ are the estimated delay and complex amplitude corresponding to the selected scatterer peak found on the array position r. Then, we go back to step B and repeat the detection process to search for the next strongest scatterer. The approach can be interpreted as a successive cancellation of the channel, at every iteration a scatterer is detected and cancelled from the channel. The process can be repeated until no more scatterers are to be detected.

IV. Experimental Verification: Outdoor Measurement Campaign

A. UWB Measurement Campaign

To test our method, we performed a UWB measurement campaign in an outdoor scenario. Fig. 1 shows a photo of the actual location, a gas station in Staffanstorp, Sweden. For every antenna position, we measured the complex channel

[2]It is important to stress that $\hat{\mathbf{d}}_r$ is a vector of peak delays for one array position and $\hat{\mathbf{d}}_r$ is a vector of scatterer delays which crosses all array positions.

Fig. 1. Photo of the measurement site, the Hydro gas station in Staffanstorp, Sweden.

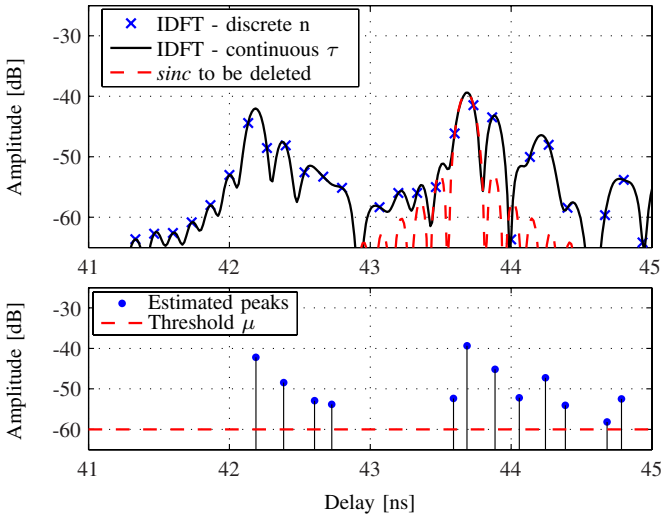

Fig. 2. (*upper*) Example of a channel impulse response after applying the Inverse Fourier Transform to the measured data. (*lower*) Estimated peaks for the same channel impulse response as above.

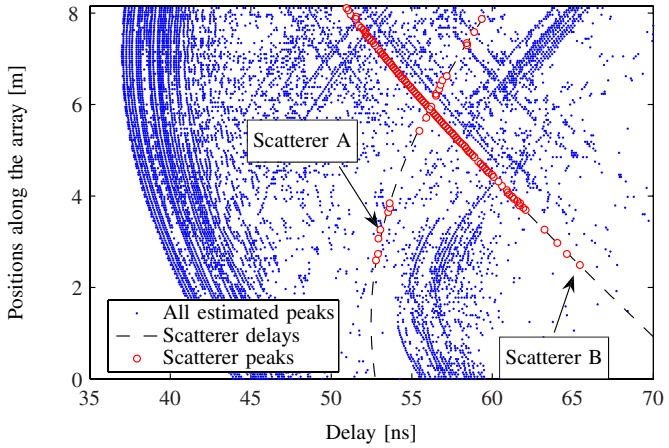

Fig. 3. View of the detected peaks form all the array positions. Only the delays of the peaks are visible, not their amplitudes.

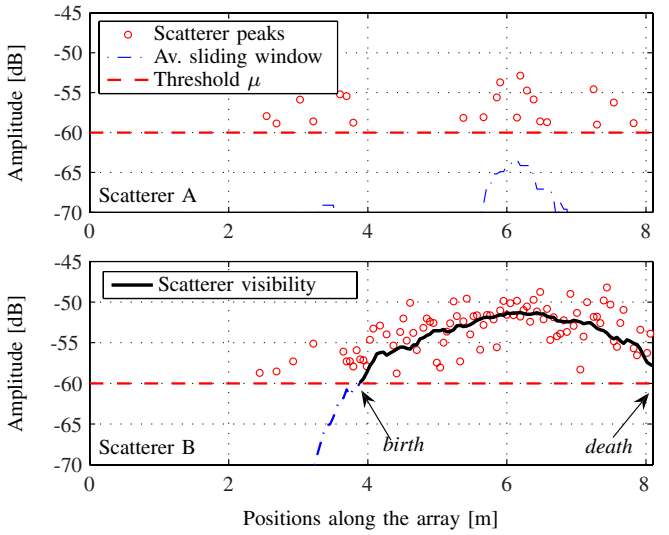

Fig. 4. Selected peak amplitudes and corresponding ASWs for scatterer A and B. The array positions without a selected peak, are considered to have zero amplitude on the ASW calculation.

coefficient of 1601 frequency points, using an HP8720C VNA, covering the frequency range 3.1-10.6 GHz. We had an LNA with 28dB gain connected to the receiver antenna to improve our signal-to-noise ratio. One of the antennas was moved along an 8 m rail, sampling the channel at 170 discrete positions separated by 48 mm ($\approx \lambda_{max}/2$). The shortest distance between the receive antenna and the virtual array of transmit antennas was 12 m. We chose to use SMT-3TO10M-A SkyCross antennas, due to their small dimensions and relatively flat frequency response of the azimuthal pattern.

B. Method Steps with Measured Data

Now, we illustrate some of the detection method steps with the measured data. Fig. 2 illustrate the peak search whereas Fig. 3 and 4 illustrate the scatterer detection.

Fig. 2 (*upper*), shows the channel impulse response from one of the transmitter positions. From it, one can realize the importance of performing the high resolution peak search formulated in (9) and (10). Considering only the discrete values of the IDFT is not enough to obtain the exact peak delays and amplitudes. Also, the same figure clearly shows the effect of the successive cancellation, when a peak is canceled, the surrounding values are significantly influenced.

Fig. 2 (*lower*), shows part of the detected peaks using the same data. Here, the threshold μ was set to 20dB below the strongest received amplitude. It is interesting to recognize that due to the successive cancellation, no peaks were detected before the line-of-sight peak, at 42.19 ns.

Fig. 3 depicts the result of detecting all the peaks above the threshold for all the array positions and plotting them together. It shows all the estimated delays stored in $\{\mathbf{d}_r\}_{r=1}^{N_R}$. In the figure we also show the results for two candidate scatterers, taken from the two-dimensional grid search. Scatterers A and B, were intentionally chosen as examples of a bad and a good candidate, respectively. Their lines of the delays correspond to the values in $\mathbf{d}_A$ and $\mathbf{d}_B$. Scatterer A has only few and sparsely selected peaks; its delays do not coincide with any

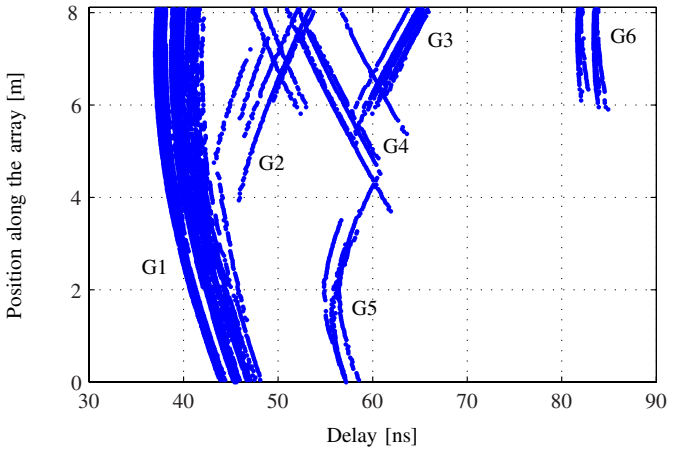

Fig. 5. Detected scatterer peaks in the delay domain (results after 60 iterations).

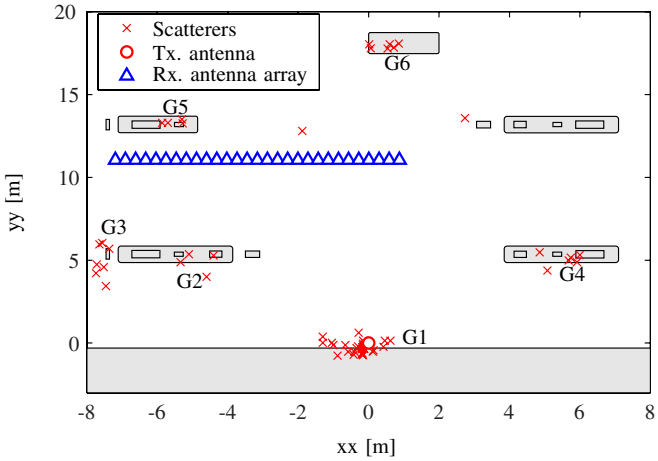

Fig. 6. Map of the measurement scenario and the calculated scatterers spatial positions. Petrol pumps and shop building are shown.

group of detected peaks. In contrast, scatterer B has many and consecutively selected peaks. It's delays coincide with a strong group of detected peaks, which probably originated from the same point in space.

Fig. 4 shows the amplitudes of the selected peaks from both scatterers, together with the corresponding ASWs. The size of the sliding window N_W was set to correspond to a distance of $\approx 10\lambda_{\max}$ (20 array positions). Most of the values on $\mathbf{a}_A$ are zero, and for that reason, the vector $\mathbf{w}_A$ never exceeds the threshold. Therefore, the weight given to scatterer A is zero. On the other hand, $\mathbf{a}_B$ has many non-zero elements and we can identify its *birth* and *death* positions. The weight of scatterer B will then be equal to the sum of the amplitudes of the peaks within its *birth* and *death* positions.

After weighting all the candidate scatterers, we choose the strongest, save its data, cancel it from the channel and repeat the detection process, accordingly to the description in III-D.

C. Results

The detected scatterers are shown both in the delay domain, Fig. 5 and in the spatial domain, Fig. 6. The detection process was stopped after detecting the 60 strongest scatterers (60 iterations). In Fig. 5 one can see the peaks corresponding to each scatterer. Fig. 6 shows the position of the antennas and the position of the most significant objects in the channel, the petrol pumps and the shop wall. Almost all the objects were identified by groups of scatterers (G#). Conversely, almost all the scatterer locations identified from the measurements correspond to physical objects. This is also a strong indication that single-scattering processes dominate in this scenario.

V. Conclusions And Future Work

We have described a method which identifies the scatterers in the delay domain and establishes the corresponding mapping to the two-dimensional spatial domain. The verification of the method with real measurement data, resulted on the successful detection of the main objects (scatterers) of the channel. This is of great value for UWB channel modeling, and the automated generation of environment maps. We propose a measurement setup that uses a single antenna position on one of the link ends and an array (route) of positions on the other. It is obvious that increasing the number of antenna positions on both ends, along new directions, would result in more accurate results. Our algorithm could be easily generalized to such a case. However even the simple version presented here already offers excellent accuracy.

The assumption in this method is that the channel is described by single bounce components, double bounces and other more complex propagation paths are not considered. Future work will be focused on a logical evolution step to include multiple reflections in our channel model and also to account for the frequency dependency of the antennas.

Furthermore, the strongest scatterer is currently found using a grid search which, in some cases, might result in a long detection process. For this reason, we will make some efforts in optimizing the grid search

VI. Acknowledgements

The financial support of the Swedish Strategic Research Foundation (SSF) Center of High Speed Wireless Communications (HSWC) at Lund University and of the Swedish Vetenskapsrådet are gratefully acknowledged.

References

[1] R. Zetik, J. Sachs, and R. S. Thomä, "Imaging of propagation environment by UWB channel sounding," in *COST 273 Bologna, Italy*, no. TD(05) 058, January 2005.

[2] G. Del Galdo, N. Czink, and M. Haardt, "Cluster spatial localization from high-resolution parameter estimation," *Proc. IEEE/ITG Workshop on Smart Antennas*, Mar. 2006.

[3] K. Haneda and J.-I. Takada, "An application of SAGE algorithm for UWB propagation channel estimation," *Ultra Wideband Systems and Technologies, 2003 IEEE Conference on*, pp. 483–487, 2003.

[4] R.-M. Cramer, R. Scholtz, and M. Win, "Evaluation of an ultra-wide-band propagation channel," *Antennas and Propagation, IEEE Transactions on*, vol. 50, no. 5, pp. 561–570, 2002.

[5] A. F. Molisch, "Ultrawideband propagation channels theory, measurement, and modeling," *IEEE Transactions on Vehicular Technology*, vol. 54, no. 5, pp. 1528–1545, 2005.

[6] C. Falsi, D. Dardari, L. Mucchi, and M. Z. Win, "Time of arrival estimation for UWB localizers in realistic environments," *EURASIP Journal on Applied Signal Processing*, Article ID 32082, 2006.